Extended Abstracts of the 2009 International Conference on Solid State Devices and Materials, Sendai, 2009, pp984-985

Performance Comparisons of Ballistic Silicon-Nanowire and Graphene Nanoribbon MOSFETs Considering First-Principles Bandstructure Effects

Haruki Ando, Shun Sawamoto, Tadashi Maegawa, Takeshi Hara, Hironobu Yao, Hideaki Tsuchiya and Matsuto Ogawa

Kobe University, Graduate School of Eng., Dept. of Electrical and Electronics Eng.
1-1, Rokko-dai, Nada-ku, Kobe 657-8501, Japan
Phone & Fax (common): +81-78-803-6082 E-mail: tsuchiya@eedept.kobe-u.ac.jp

1. Introduction

Silicon nanowire (SNW) and graphene nanoribbon (GNR) transistors have much attention due to high injection velocity in [110]-oriented silicon nanowire [1] and ultra-high electron mobility in bulk graphene [2]. In this paper, we investigate performance potentials of SNW and semiconducting GNR MOSFETs, by using the first-principles bandstructures and ballistic current estimation based on the "top-of-the-barrier" model [3]. As a result, we found that the [110]-oriented SNW transistors (SNWT) provide smaller intrinsic device delays than the Si ultrathin-body (UTB) MOSFETs, and furthermore the GNR transistors (GNRT) outperform both the Si-UTB MOSFETs and the [110] SNWTs, if a few nanometer ribbon widths can be achieved.

2. Bandstructures

Fig. 1 shows the atomic models used in the simulation, where we also considered Si-UTB structure shown in Fig. 1 (a), which gives an upper limit performance of the conventional planar Si-MOSFETs under unstrained condition. The square-shaped SNWs with two different orientations, [110] and [100], are investigated as shown in Figs. 1 (b) and (c), since they exhibit better performance than other orientations [1]. For GNR, we focus only on armchair-edged GNR shown in Fig. 1 (d), which is known to become semiconducting under certain condition and therefore appears to be promising for FET applications [4]. Fig. 2 shows the bandstructures computed by using a first principles simulation package based on the density-functional theory, VASP [5], where the electron-electron exchange and correlation interactions were treated within the generalized gradient approximation (GGA). It is found that all the bandstructures have direct bandgap [1,4,6]. Note that the length of the first-Brillouin zone is different among the four structures, because of different unit cell size in the orientations considered. In Fig. 2 (d), the dispersion curves for W=2.1nm (N=18) and W=4.3nm (N=36) are simultaneously plotted, which tell us that effective mass both of electron and hole reduces with increasing W, though the bandgap energy significantly decreases [4].

Next, Fig. 3 shows the wire width and UTB thickness dependences of the electron effective mass for Si-UTB and SNWs. It is found that the Si-UTB structure has almost the same effective mass as the bulk m_t, down to the sub-1nm thickness. On the other hand, the [110] SNW has smaller effective mass as ~$0.13m_0$ [1,6], while the mass of the [100] SNW increases drastically with downsizing [1]. The above effective mass variations in the SNWs will influence a device performance as discussed later. The electron effective mass of the GNR also increases with decreasing W as shown in Fig. 4 (a) for both N=3m and 3m+1, where m is an integer. For armchair-edged GNRs, the bandstructure is known to be metallic when N=3m-1 [4]. Based on the results of Fig. 4 (a), GNRs with larger ribbon widths will help to increase electron velocity due to smaller effective mass, but the GNR width should become below a few nanometers to make the bandgap energy acceptable for the FET operation [4], as found in Fig. 4 (b).

3. Electrical Properties

By using the first-principles bandstructures, we computed electrical properties of SNWTs and GNRTs as shown in Figs. 5 and 6, which were computed based on the ballistic "top-of-the-barrier" model [3]. The simulations are performed at the same OFF-current (I_{off}=0.1nA). It is found from Fig. 5 (a) that the [110] SNWTs have larger drain current than the [100] ones, which is due to the smaller effective masses as reported in Fig. 3. As a result, faster switching operation, even faster than the Si-UTB devices, is expected in the [110] SNWTs as shown in Fig. 5 (b). Interestingly, the [110] SNWT with W=1.55nm (■) exhibits the fastest operation. Furthermore, from Fig. 6 the GNR with W=4.3nm (▷) is found to outperform such [110] SNWTs. This is due to an appearance of the steeply linear dispersion curve in the case of W=4.3nm as shown in Fig. 7, which provides higher velocity than the [110] SNWTs, even though the effective masses at the conduction band minimum are comparable.

4. Conclusions

We have investigated the device performances of SNW and GNR MOSFETs by using the first-principles bandstructures and the ballistic current model. As a result, we found that the [110]-oriented SNW and the GNR transistors are promising candidates as digital switches, if a few nanometer wire and ribbon widths can be well achieved.

Acknowledgements

This work was supported by the Semiconductor Technology Academic Research Center (STARC).

References [1] N. Neophytou et al., IEEE TED-55 (2008) 1286. [2] K. Bolotin et al., Solid State Comm. 146 (2008) 351. [3] A. Rahman et al., IEEE TED- 50 (2003) 1853. [4] G. Liang et al., IEEE TED-54 (2007) 677. [5] G. Kresse et al., PRB-54 (1996) 11169. [6] T. Maegawa et al., IEEE TED- 56 (2009) 553.

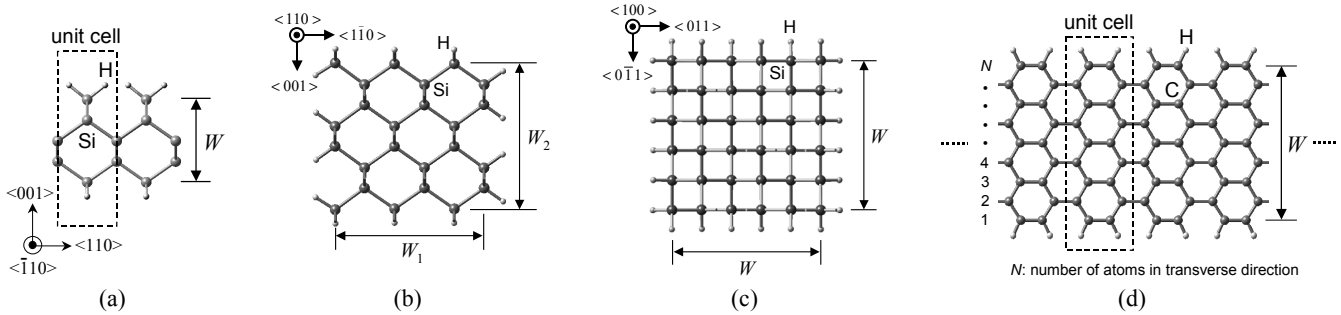

Fig. 1 Atomic models used in the simulations for (a) Si-UTB, (b) [110] SNW, (c) [100] SNW, and (d) armchair-edged GNR. Hydrogen atoms are assumed to eliminate surface dangling bonds. The dashed rectangles in (a) and (d) denote each unit cell.

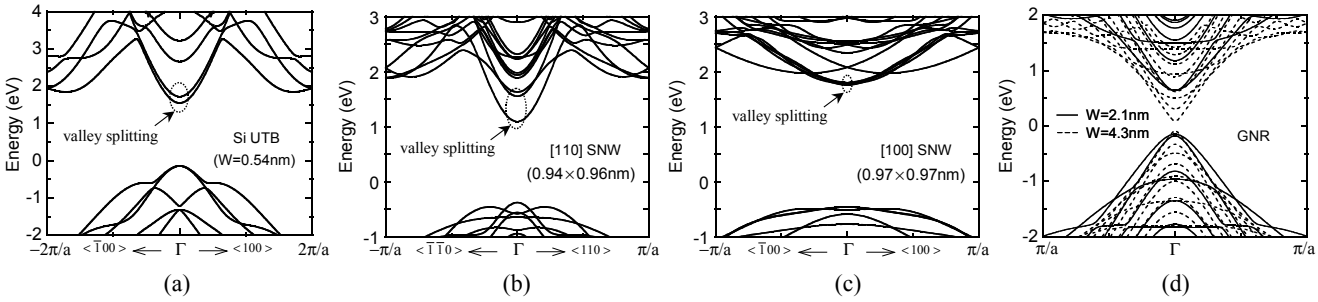

Fig. 2 Bandstructures computed for (a) Si-UTB, (b) [110] SNW, (c) [100] SNW, and (d) GNR. Sizes are indicated in each figure.

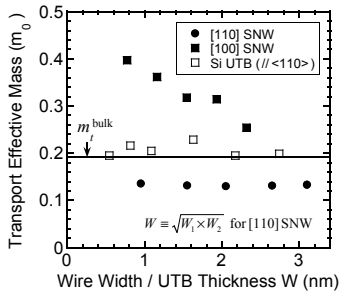

Fig. 3 Size dependences of electron effective mass for Si-UTB, [110] SNW and [100] SNW.

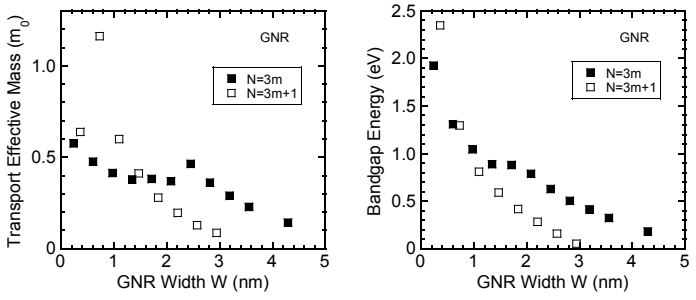

Fig. 4 Ribbon width dependences of (a) electron effective mass and (b) bandgap energy for GNR. As is well-known, the bandgap energy is underestimated in the present calculations based on the density-functional theory.

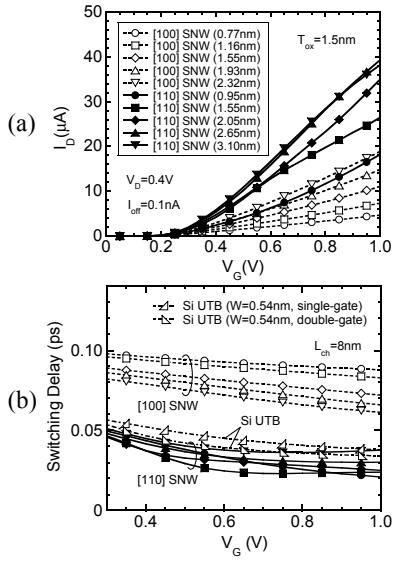

Fig.5 Comparisons of (a) I_D-V_G characteristics and (b) intrinsic device delays computed for [110]- and [100] SNWTs. In (b), the results for Si-UTB devices are also plotted. The symbols for SNWs in (b) coincide with those in (a).

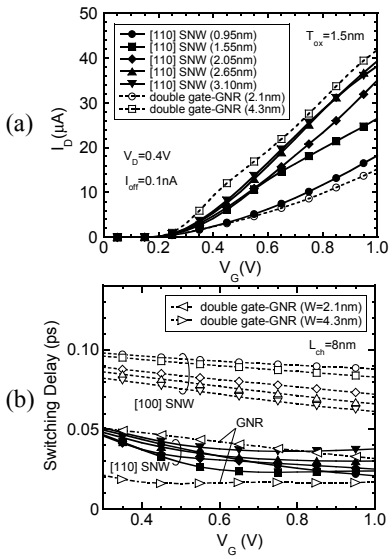

Fig. 6 Comparisons of (a) I_D-V_G characteristics and (b) intrinsic device delays computed for [110] SNWTs and GNRTs. In (b), the results for [100] SNWTs are also plotted. The symbols for SNWs coincide with those in Fig. 5.

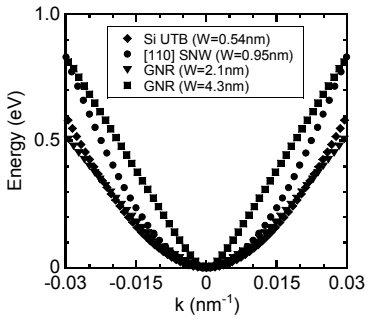

Fig. 7 Comparison of conduction band dispersion curves at Γ point for Si-UTB, [110] SNW and GNRs with W=2.1nm and 4.3nm. The conduction band minimum energy was set at zero for all cases.